

High-Gain Direct-Drive Target Designs for the National Ignition Facility

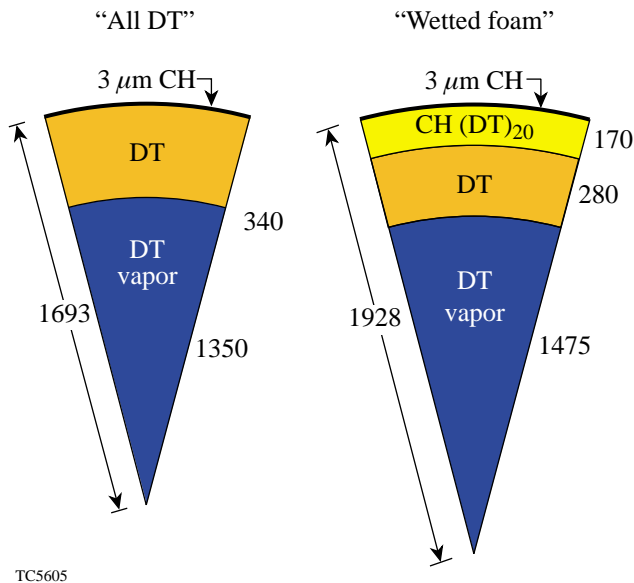
Introduction

Direct drive¹ offers the potential of higher target gain for the National Ignition Facility (NIF)² than indirect drive.³ Direct-drive targets have been designed that reach a gain of 45 in one-dimensional (1-D) simulations using primarily a pure cryogenic DT shell driven on an isentrope where the pressure is three times the Fermi-degenerate pressure ($\alpha=3$). The sensitivity of this design to laser and target-surface nonuniformities has been studied with two-dimensional (2-D) simulations.⁴ At the levels of nonuniformity expected for the NIF, the neutron yield was calculated to be about 70% of the 1-D value, producing a target gain of 30. A second class of targets has the potential of achieving even higher gain. In these designs, the outer portion of the cryogenic DT shell is replaced with a region of low-density CH foam. Liquid DT is “wicked” into the voids of the foam.⁵ The advantage of these “wetted-foam” designs over the “all-DT” target is that the presence of higher-Z material (C) in the laser deposition region results in increased laser absorp-

tion. For the NIF designs, the laser absorption increases by ~40% (going from 60% absorption in DT to 85% in the wetted foam). For a scaled-down version of the wetted-foam target, which can be examined on LLE’s OMEGA laser, the laser absorption is increased by almost a factor of 2, effectively doubling the amount of energy available to drive the target. With the increased laser energy, the capsules can contain an increased amount of fuel. The wetted-foam targets are thicker, providing increased stability, and the additional fuel provides higher neutron yield.

Results–NIF

A comparison between one possible wetted-foam design for the NIF and the base-line “all-DT” design is shown in Fig. 88.15, with the targets drawn approximately to scale. (In Fig. 88.15 and the other figures, distances are labeled in microns and IFAR is the in-flight aspect ratio.) The main result is that the wetted-foam design achieves a 1-D target gain that



1.5-MJ Designs		
	All DT	Wetted foam
Gain	45	120
Absorption (%)	60	85
ρR (g/cm ²)	1.3	1.7
Adiabat (α)	3	2
Peak IFAR	60	50
Margin	44	32

Figure 88.15

Comparison between the wetted-foam and all-DT direct-drive target designs for the NIF. The wetted-foam design has ~40% higher laser absorption and more than twice the target gain.

is almost three times higher than the gain for the all-DT target. Most of this large increase in target gain is directly related to the increase in target size. The foam target is about 30% thicker, its outer diameter is about 20% larger, and it contains about 80% more fuel. Since the foam target is thicker, it can be driven on a lower adiabat ($\alpha=2$) than the all-DT target ($\alpha=3$), without compromising shell integrity during the acceleration phase of the implosion. This, combined with the larger fuel mass, results in a 30% increase in the peak areal density ρR (where ρ is the density and R is the radius) achieved by the fuel (1.85 versus 1.3 g/cm²). The fraction of fuel burned (or *fractional burnup*) by thermonuclear reactions is roughly proportional to the peak ρR (in this range). The 80% increase in fuel mass combined with a 30% increase in fractional burnup of the fuel increases the target gain by a factor of 2.5 and accounts for most of the increased gain shown in Fig. 88.15.

A preliminary stability analysis of the wetted-foam design shows that this target is more stable than the all-DT target during the acceleration phase of the implosion. Figure 88.16 shows the result of applying a stability postprocessor⁶ to the 1-D simulations for these targets. The shell thickness and the size of the mixed region resulting from hydrodynamic instabilities are plotted as functions of time. Both simulations use the same “seeds” for the Rayleigh–Taylor instability caused by laser-beam nonuniformity and target-surface roughness. In these simulations the foam is treated as a homogeneous material. The shell size is four times larger than the mix region for the foam target and three times larger for the all-DT target. This improved margin for stability of the foam design is mainly the result of the increased thickness of the target shell.

A similar stability analysis for the deceleration phase of the implosion showed that the fractional distortion of the hot spot was significantly larger for the foam target than for the all-

DT target. This was the result of a lower implosion velocity for the foam target than for the all-DT target: 3×10^7 cm/s versus 4×10^7 cm/s. Because of the lower implosion velocity, the target decelerates for a longer time before the ignition temperature is reached. Lower temperatures during deceleration also reduce the ablative stabilization of the Rayleigh–Taylor growth.⁷ These two factors—increased deceleration time before ignition and increased growth rates—result in increased distortion of the hot spot even though the initial seed for deceleration growth is somewhat smaller for the foam design. These stability estimates will be verified with multidimensional simulations.

To achieve greater stability during the deceleration phase, a second foam design with a higher implosion velocity has been developed. This design (target #1 in Fig. 88.17) is smaller, has a thinner shell, and is less massive than the higher-gain wetted-foam design (target #2 in Fig. 88.17) in order to achieve the higher velocity. The foam density was increased from 30 mg/cm³ to 140 mg/cm³ to maintain high laser absorption for the smaller target. Because the target is thinner, the adiabat had to be increased from $\alpha = 2.0$ to $\alpha = 2.5$ to maintain sufficient stability during the acceleration phase of the implosion. The penalty paid for the increased stability was a reduction in target gain due to the higher adiabat and smaller amount of fuel. Nonetheless, the 1-D target gain for this foam design is still almost a factor of 2 higher than for the all-DT gain: 80 versus 45. A stability analysis for both the acceleration and deceleration portions of the implosion shows distortion comparable to that of the all-DT design, which was calculated to achieve 70% of the 1-D yield.

Results—OMEGA

The high-velocity, wetted-foam design was scaled down to 35 kJ to examine what experiments could be performed using

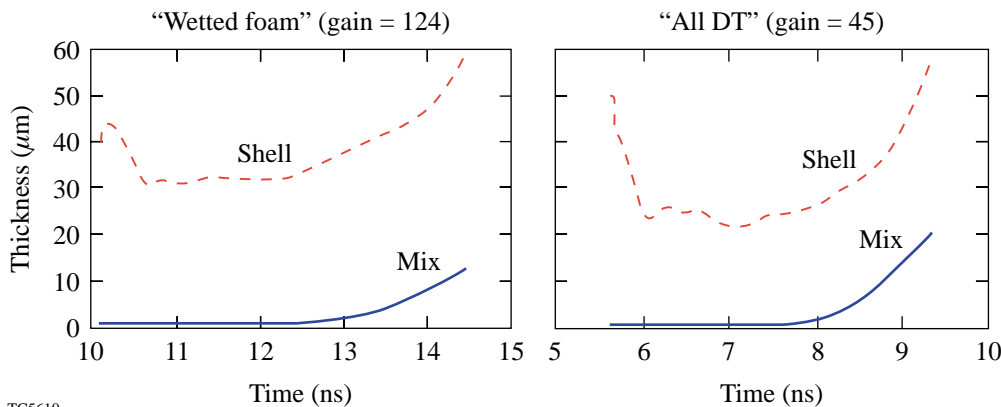
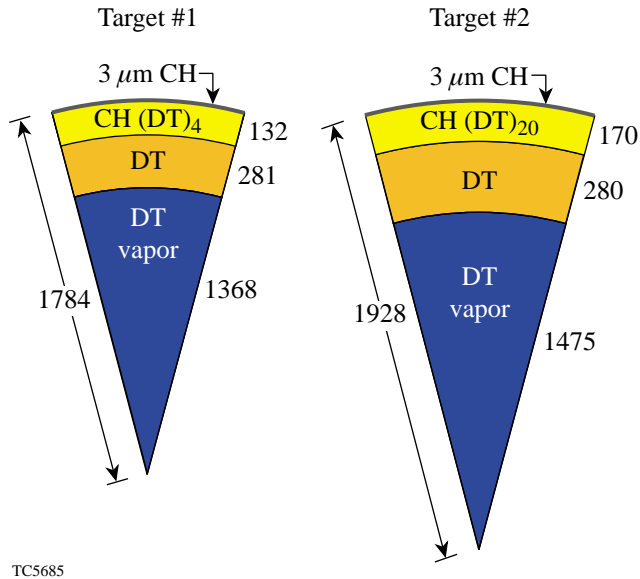


Figure 88.16
Shell thickness and mix thickness as a function of time during the acceleration phase of the implosion for the wetted-foam and all-DT designs shown in Fig. 88.15.

TCS610

the OMEGA laser. The design was tuned to achieve a target gain of 0.3 with the highest-possible adiabat (for maximum stability during acceleration) and the highest-possible implosion velocity (for the maximum stability during deceleration). The target and pulse shape are shown in Fig. 88.18. A target gain in the range of 0.2 to 0.3 would demonstrate the onset of bootstrap heating. Bootstrap heating is the self-heating process whereby alpha particles from the DT reaction deposit their energy back into the fuel and raise the temperature, resulting in a significant increase in the thermonuclear reaction rate. To be

effective, the region of neutron production (hot spot) should be comparable in size to the distance over which alpha particles lose their energy. This corresponds to a ρR of $\sim 300 \text{ mg/cm}^2$. This 35-kJ, wetted-foam design shows a measurable amount of bootstrap heating. The effect of bootstrap heating is seen in Fig. 88.19, which shows the computed neutron yield plotted as a function of variations in the length of the foot of the laser pulse. For the optimal foot length, the neutron yield is highest due to optimal timing of the shocks in the target. To see the effect of bootstrap heating, a second curve in Fig. 88.19 shows

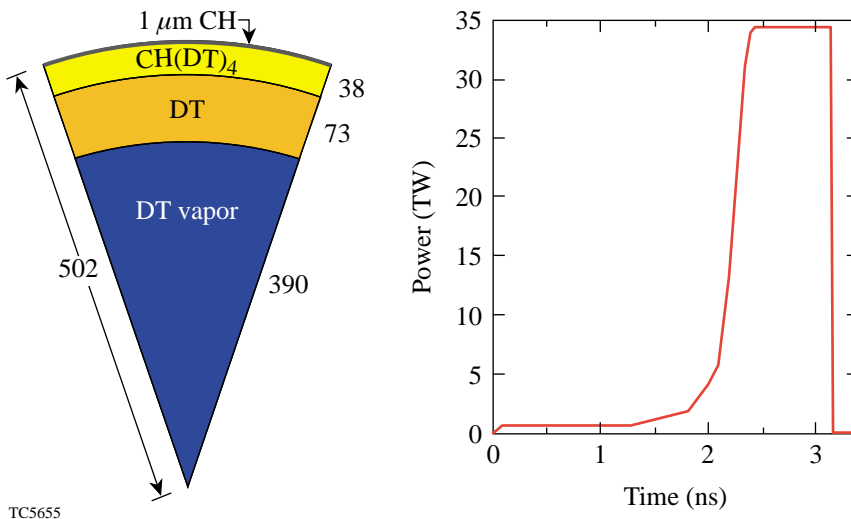


	1.5-MJ Wetted-Foam Designs	
	Target #1	Target #2
Foam (mg/cm^3)	140	30
Gain	81	120
Absorption (%)	90	85
ρR (g/cm^2)	1.4	1.7
Adiabat	2.5	2.0
Margin	48	32
Velocity (cm/s)	4.0×10^7	3.2×10^7

TC5685

Figure 88.17

Comparison between two wetted-foam designs for the NIF. The smaller target has a higher implosion velocity, resulting in greater stability during the deceleration phase of the implosion.



TC5655

Figure 88.18

A 35-kJ wetted-foam design for experiments on the OMEGA laser. This target is a scaled-down version of the smaller target illustrated in Fig. 88.17.

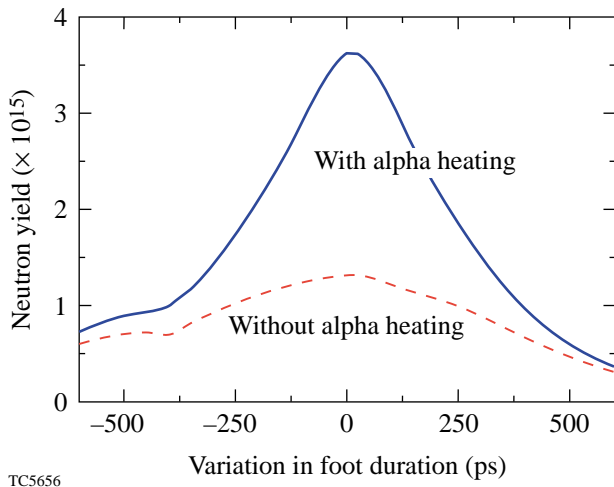


Figure 88.19 The effect of bootstrap heating on neutron yield. Neutron yield is plotted as a function of the length of the foot of the pulse shown in Fig. 88.18. For the optimal pulse length, there is an optimal coalescence of shocks within the fuel, resulting in maximum neutron production. At maximum neutron production there is enough alpha-particle heating of the fuel that the neutron yield is a factor of 3 higher than it would be without this heating.

the neutron yield with alpha-particle heating turned off in the simulation. Under these conditions alpha heating increases the neutron yield by a factor of ~3 at optimal shock timing when the neutron production is largest. Moving away from peak neutron production, the amount of alpha heating becomes too small to significantly increase the temperature. The density and temperature profiles in the fuel at one instant in time during neutron production are shown in Fig. 88.20. The hot region extends close to a ρR of 300 mg/cm^2 , which is the expected condition for bootstrap heating.

To observe these effects on OMEGA, improvements in laser uniformity and target quality are required. The levels of nonuniformity from target-surface roughness and laser nonuniformity would have to be typically a factor of 2 to 4 smaller than required for the NIF because the OMEGA targets are about 3.5 times smaller. An initial stability analysis of this target was performed using a stability postprocessor.⁶ We used a $0.5\text{-}\mu\text{m}$ inner-surface roughness for the DT ice and the laser imprint corresponding to SSD with 1-THz bandwidth and two color cycles and twice the spectral dispersion that is currently used on OMEGA to seed the Rayleigh–Taylor instability from target-surface roughness and laser nonuniformity. These specifications for the laser and target uniformities are beyond

current capabilities on OMEGA, but they should be achievable with extensions of current technology. A plot of shell thickness and mix thickness is shown in Fig. 88.21. At the time of closest approach, the shell is twice as large as the mixed region. This might be adequate but will have to be examined with two-dimensional simulations.

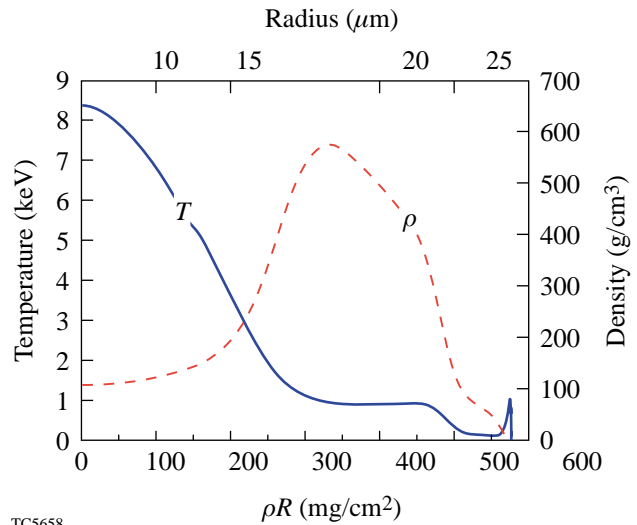


Figure 88.20 Density and temperature profiles at one instant in time during neutron production. The temperature and density profiles of the hot region are characteristic of hot-spot conditions in an igniting target.

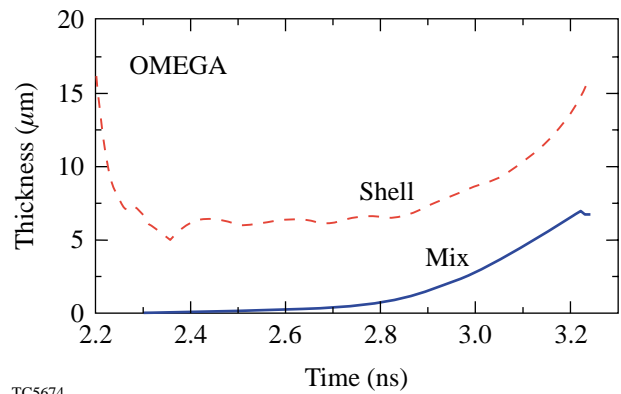


Figure 88.21 Shell thickness and mix thickness as a function of time for the OMEGA wetted-foam design (from Fig. 88.18) during the acceleration phase of the implosion. The laser nonuniformity was a factor of 2 lower than currently achieved on OMEGA, and an inner-surface roughness of $0.5 \mu\text{m}$ was used.

The design presented here will be scaled down to the lower energies (25 to 30 kJ) that can be expected on OMEGA for pulse shapes similar to that shown in Fig. 88.18. While the signal of bootstrap heating will be less dramatic than that shown in Fig. 88.19, the demonstration that this new type of target can be successfully imploded with a greatly increased laser absorption would be an exciting result with significant implications for direct-drive NIF designs. A program for developing the key areas necessary for wetted-foam implosions is being developed. This includes an investigation of the feasibility of fabricating foam shells of the required quality.

ACKNOWLEDGMENT

This work was supported by the U.S. Department of Energy Office of Inertial Confinement Fusion under Cooperative Agreement No. DE-FC03-92SF19460 and the University of Rochester. The support of DOE does not constitute an endorsement by DOE of the views expressed in this article.

REFERENCES

1. J. Nuckolls *et al.*, *Nature* **239**, 139 (1972).
2. M. D. Campbell and W. J. Hogan, *Plasma Phys. Control. Fusion* **41**, B39 (1999).
3. S. E. Bodner, D. G. Colombant, J. H. Gardner, R. H. Lehmborg, S. P. Obenschain, L. Phillips, A. J. Schmitt, J. D. Sethian, R. L. McCrory, W. Seka, C. P. Verdon, J. P. Knauer, B. B. Afeyan, and H. T. Powell, *Phys. Plasmas* **5**, 1901 (1998).
4. P. W. McKenty, V. N. Goncharov, R. P. J. Town, S. Skupsky, R. Betti, and R. L. McCrory, *Phys. Plasmas* **8**, 2315 (2001).
5. R. A. Sacks and D. H. Darling, *Nucl. Fusion* **27**, 447 (1987).
6. V. N. Goncharov, P. McKenty, S. Skupsky, R. Betti, R. L. McCrory, and C. Cherfils-Clérouin, *Phys. Plasmas* **7**, 5118 (2000).
7. V. Lobatchev and R. Betti, *Phys. Rev. Lett.* **85**, 4522 (2000).